Matter and Radiation at Extremes | RESEARCH ARTICLE | scitation.org/journal/mre

Photonuclear production of medical isotopes ^{62,64}Cu using intense laser-plasma electron source

Cite as: Matter Radiat. Extremes 4, 064401 (2019); doi: 10.1063/1.5100925
Submitted: 22 April 2019 • Accepted: 11 August 2019 •
Published Online: 24 September 2019

ZhiGuo Ma,[1] HaoYang Lan,[1] WeiYuan Liu,[2] ShaoDong Wu,[1] Yi Xu,[3] ZhiChao Zhu,[1] and Wen Luo[1,a)]

AFFILIATIONS

[1]School of Nuclear Science and Technology, University of South China, 421001 Hengyang, People's Republic of China
[2]Key Laboratory for Laser Plasmas (Ministry of Education) and School of Physics and Astronomy, Shanghai Jiao Tong University, Shanghai 200240, People's Republic of China
[3]Extreme Light Infrastructure–Nuclear Physics, RO-077125 Magurele, Romania

[a)]**Author to whom correspondence should be addressed:** wenluo-ok@163.com

ABSTRACT

^{62,64}Cu are radioisotopes of medical interest that can be used for positron emission tomography (PET) imaging. Moreover, ^{64}Cu has β^- decay characteristics that allow for targeted radiotherapy of cancer. In the present work, a novel approach to experimentally demonstrate the production of ^{62,64}Cu isotopes from photonuclear reactions is proposed in which large-current laser-based electron (e^-) beams are generated from the interaction between sub-petawatt laser pulses and near-critical-density plasmas. According to simulations, at a laser intensity of 3.4×10^{21} W/cm^2, a dense e^- beam with a total charge of 100 nC can be produced, and this in turn produces bremsstrahlung radiation of the order of 10^{10} photons per laser shot, in the region of the giant dipole resonance. The bremsstrahlung radiation is guided to a natural Cu target, triggering photonuclear reactions to produce the medical isotopes ^{62,64}Cu. An optimal target geometry is employed to maximize the photoneutron yield, and ^{62,64}Cu with appropriate activities of 0.18 GBq and 0.06 GBq are obtained for irradiation times equal to their respective half-lives multiplied by three. The detection of the characteristic energy for the nuclear transitions of $^{62,\ 64}$Cu is also studied. The results of our calculations support the prospect of producing PET isotopes with gigabecquerel-level activity (equivalent to the required patient dose) using upcoming high-intensity laser facilities.

I. INTRODUCTION

^{64}Cu [$T_{1/2}$ = 12.7 h; β^+ decay with 278 keV mean energy (17.6%); β^- decay with 191 keV mean energy (38.5%); low-energy Auger electrons] has decay characteristics that allow for positron emission tomography (PET) imaging and targeted radiotherapy of cancer.[1–3] ^{64}Cu-ATSM is an imaging agent used for measuring hypoxia in human tumors. Hypoxia is an important effect that can influence the resistance of tumor cells to chemo- or radiotherapy.[4] ^{62}Cu is a relatively short-lived β^+ emitter [$T_{1/2}$ = 9.67 min; β^+ decay with 1.32 MeV mean energy (97.6%)] that is very suitable for PET imaging.[1–3] Moreover, ^{62}Cu can form a "matched pair" with ^{64}Cu. Note that a β^- (or Auger electron) and β^+ emitting pair of radionuclides of the same element is now termed a theranostic pair[1] and represents a new frontier in the field of nuclear medicine.

At present, ^{64}Cu is mainly produced using small cyclotrons with the ^{64}Ni(p, n) and ^{64}Zn(d, 2p) reactions, as well as in nuclear reactors with the ^{63}Cu(n, γ) reaction.[5–8] On the other hand, ^{62}Cu is commonly produced from ^{62}Zn/^{62}Cu generators, and the parent isotope ^{62}Zn can be obtained by the ^{63}Cu(p, 2n) reaction in a cyclotron.[8–11] Generally, cyclotron-based radioisotope production requires large proton capture cross sections, while radioisotope production by reactor methods needs large fission branching ratios. Furthermore, nuclear reactors lead to large amount of nuclear waste, raising numerous safety and security concerns. Cyclotrons may not pose such risks compared with nuclear reactors, but they produce only a limited range of isotopes for clinical use.[12] In addition to their reasonable half-lives, accelerator-produced neutron-deficient isotopes have relatively high purity and specific activity. Thus, to a certain extent, accelerator production of isotopes represents a favorable option for medical applications.[2] However, owing to the limited number of production facilities available and the growing global demand for medical isotopes, there is a potential crisis in terms of global under-supply.[13,14] It is therefore vital to explore innovative ways of producing medical isotopes without nuclear reactors.

Recent progress in laser technology, including chirped pulse amplification (CPA) and optical parametric CPA (OPCPA) has

stimulated global interest in the development of high-peak-power lasers.[15] Such lasers can be focused to peak intensities of the order of 10^{20} W/cm^2.[16,17] Hence, they can be employed to study various nuclear phenomena,[18,19] including the production of key medical isotopes. Fritzler *et al.*[20] have calculated that 13 MBq of ^{11}C can be generated, via (p, n) reaction, using the LOA tabletop laser after 30 min irradiation at 10 Hz. Ledingham *et al.*[21] have demonstrated laser-driven ^{11}C and ^{18}F PET isotope production with the high-power VULCAN laser at the Rutherford Appleton Laboratory (RAL), UK. Photonuclear reactions provide an alternative method for the production of medical isotopes. As an example, for producing ^{64}Cu, the ^{65}Cu(γ, n) channel does not require a rare and expensive ^{64}Ni target or a chemical separation step, which makes it advantageous for medical isotope production. However, an energetic γ-ray beam with sufficient brilliance is still required in order to produce radioisotopes with sufficient activity.

In this paper, an efficient photonuclear scheme is proposed to produce radioisotopes of medical interest by using high-charge relativistic e^- beams. Such e^- beams are produced from the interaction between an intense laser pulse and a near-critical-density (NCD) plasma. Taking ^{62}Cu as an example, a photonuclear scheme for producing PET isotopes is illustrated schematically in Fig. 1. By focusing the electrons onto a high-Z target such as tantalum, energetic γ-rays are produced through bremsstrahlung radiation. These γ-rays in turn induce photonuclear reactions inside the Cu sample. The (γ, n) reaction is the main reaction that occurs, and the stable isotope ^{63}Cu can be effectively transformed into the short-lived isotope ^{62}Cu. The particle-in-cell (PIC) code EPOCH[22] is used to simulate the laser-plasma interaction, and the Monte Carlo (MC) code Geant4-GENBOD[23,24] is then used to model the passage of the particles through matter.

II. SIMULATION SETUP AND RESULTS

As early as 1995, Modena *et al.*[25] reported relativistic e^- beams produced by an intense laser pulse. More recently, Yan *et al.*[26] demonstrated that intense laser interaction with an NCD plasma could generate energetic and dense e^- beams. We have previously shown that such e^- beams could be used to efficiently transmute long-lived nuclear waste.[27,28] In this section, we first use PIC simulations to investigate the generation of high-current e^- beams from an NCD target, and we then use MC calculations to study the subsequent production of bremsstrahlung radiation and the photonuclear isotopes ^{62,64}Cu.

A. High-charge energetic e^- beam

We first perform full three-dimensional (3D) PIC simulations of ultra-intense laser pulses interacting with gas jets. A sub-petawatt p-polarized laser pulse with Gaussian spatial and temporal profiles, a wavelength of 1 μm, a duration of 33 fs, and a focal spot size of 3.0 μm at FWHM irradiates a gas region from the left. The laser intensity of 3.4×10^{21} W/cm^2 corresponds to a laser peak power of 350 TW. This peak power is far above the critical power of laser self-focusing in an NCD plasma. As a consequence, efficient electron acceleration can be obtained within almost the entire plasma region, which results in the production of dense e^- beams with cutoff energy higher than 100 MeV, as discussed below. The simulation box is 80 μm in the longitudinal (x) direction and 30 μm in the transverse (y and z) directions. Eight macro-electrons and two macro-protons are initialized in each cell, the dimensions of which are dx = 80 nm and dy = dz = 125 nm. The plasma region, of thickness 50 μm, is located at 10–60 μm. A wide range of plasma density, $n_e = (0.1–2.0)n_c$, is used in the simulation, where n_c is the plasma critical density.

The interaction between laser pulse and NCD plasma can be divided into injection and acceleration stages. The injection stage terminates at $t = 30T_0$, where T_0 is the light period. After the laser pulse hits the target surface, background electrons in the plasma are expelled from the axis of the laser by the transverse pondermotive force. This leads to a symmetric pattern of electron density, and a bubble-like structure appears near the target surface [see Fig. 2(a)]. Meanwhile the ions are hardly affected, and a strong transverse quasistatic electric field is formed because of the effective charge separation. Subsequently, a large number of electrons are captured at the rear of the bubble, forming an over-critical-density e^- beam, as shown in Fig. 2(b). Such a dense e^- beam can generate a strong radial electric field, which prevents injection of the rest of the electrons. In the following stage of acceleration, the bubble-like structure gradually evolves into a plasma channel, and the injected electrons gain energy from the strong laser field and the longitudinal quasistatic electric field inside the channel [Figs. 2(c) and 2(d)].

Figure 3(a) shows the spectral distributions of e^- beams accelerated in the NCD plasma. These spectra are broadband and

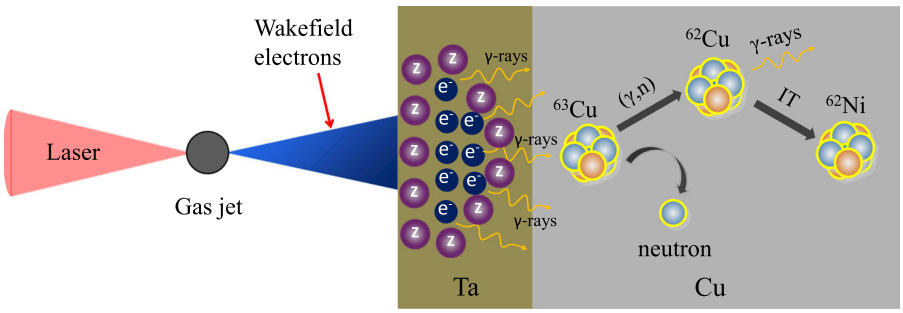

FIG. 1. Schematic illustration of ^{62}Cu isotope production. Quasicollimated e^- beams are produced from the interaction of the intense laser beam with the gas jet, and energetic bremsstrahlung photons are then generated efficiently from the Ta target irradiated by the laser-plasma-accelerated e^- beams. ^{62}Cu isotope production is realized in the following stage by irradiating a centimeter-scale Cu target with high-energy bremsstrahlung photons, inducing possible photonuclear reactions. A 2-mm-thick Ta plate is placed 2 cm downstream of the gas jet.

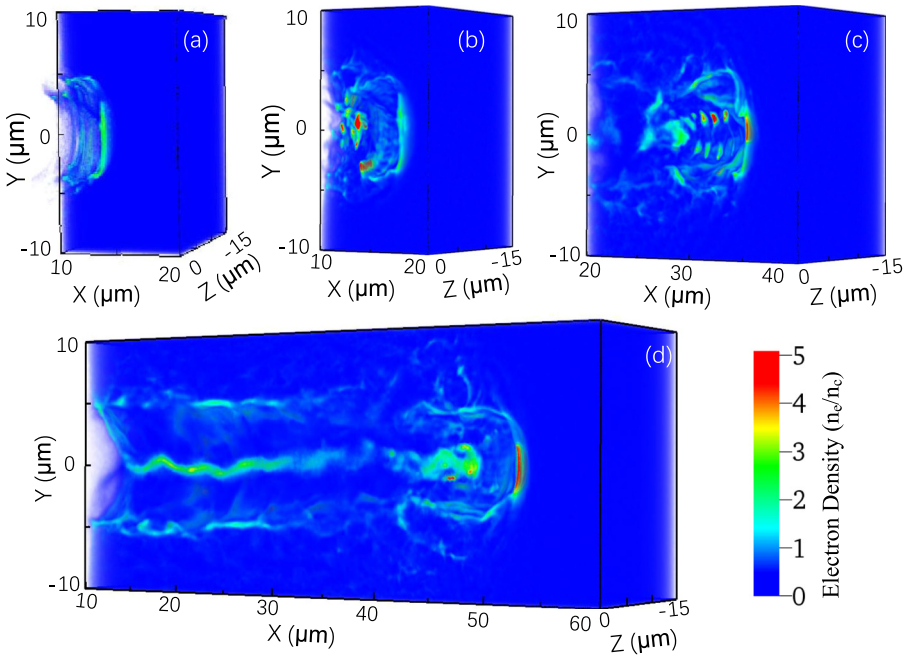

FIG. 2. Spatial profiles of the electron density at (a) $t = 15T_0$, (b) $20T_0$, (c) $40T_0$, and (d) $60T_0$. A plasma density of $n_e = 0.5n_c$ was used in the simulations.

have endpoint energy of the order of 100 MeV. Moreover, the cutoff energy increases with increasing plasma density and reaches a maximum value of 220 MeV at $n_e = 0.8n_c$. The e^- beams produced from the NCD plasma are collimated. Figure 3(b) shows the transverse profile of an e^- beam with energy higher than 6 MeV. From the spot size of the e^- beam and the transport distance from the accelerator exit to the convertor surface, the divergence angle of the e^- beam is found to be ~15°.

The electric charges of accelerated e^- beams for different plasma densities are shown in Fig. 4. Electrons with energy above the giant dipole resonance (GDR) region (≥25 MeV) dominate over those in the GDR region (10–25 MeV). Moreover, the number of electrons above the GDR region first increases and then decreases with increasing plasma density, while the number in the GDR region shows a clear opposite trend. In this study, the plasma density of $0.5n_c$ is considered to be the optimal density, leading to maximum production of high-energy electrons. At $n_e = 0.5n_c$, an e^- beam with a total charge exceeding 100 nC can be produced, with relativistic electrons (≥10 MeV) carrying an electric charge exceeding 13 nC.

B. High-flux bremsstrahlung γ-ray source

The interactions between the energetic e^- beams and the bremsstrahlung convertor, as well as the consequent medical isotope

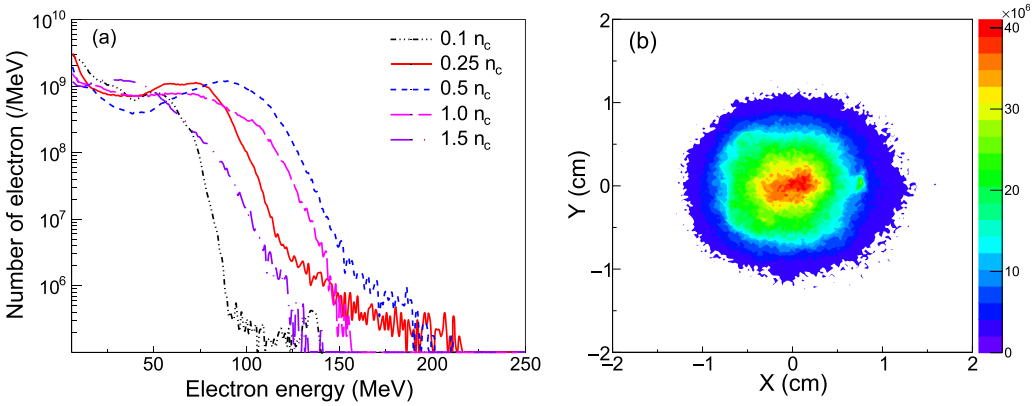

FIG. 3. (a) Energy spectra of accelerated e^- beams as functions of the density of the NCD plasma. (b) Transverse profile of e^- beam recorded on the front surface of the Ta convertor. The plasma density is set to $0.5n_c$, and the transport distance of the e^- beam from the accelerator exit to the front surface of the Ta converter is 2 cm.

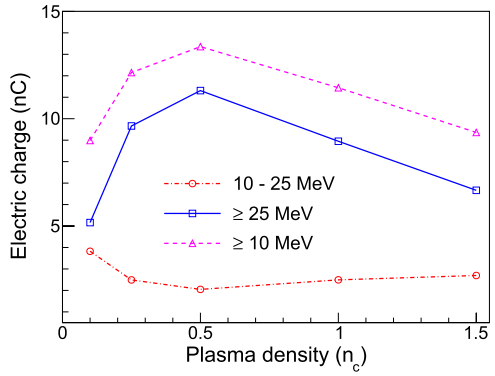

FIG. 4. Electric charge of high-energy electrons as a function of the plasma density.

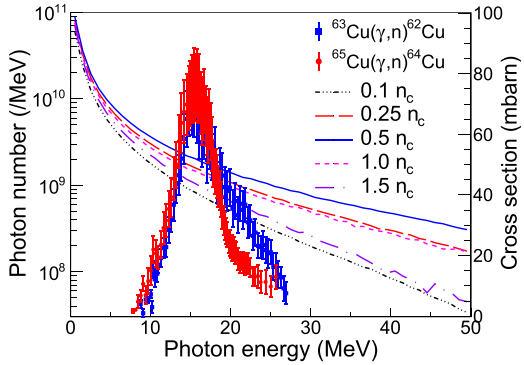

FIG. 5. Bremsstrahlung spectra for different plasma densities, together with the cross section on ^{63,65}Cu(γ, n) reactions.[30] The radius and thickness of the Ta convertors are set to 2 cm and 2 mm, respectively.

production, are investigated using the Geant4-GENBOD code,[23,24] in which the hadronic interaction module describing the photoneutron reaction process is self-consistently included. Bremsstrahlung radiation is produced by the deceleration of energetic electrons inside the convertor. Neglecting changes in the electron bunch during its propagation in the target, the differential bremsstrahlung cross section is integrated as[29]

$$\frac{d\sigma_\gamma}{dE_\gamma} = aZ^2\left(E_\gamma^{-1} - bE_e^{-1}\right), \tag{1}$$

where Z is atomic number, a = 11 mb, and b = 0.83. The number of bremsstrahlung photons radiated per mega electron volt at photon energy E_γ is evaluated as

$$\frac{dN_\gamma}{dE_\gamma} \approx d_c n_c \int_{E_\gamma}^{E_{\rm cut}} \frac{dN_e}{dE_e}\cdot\frac{d\sigma_\gamma}{dE_\gamma}dE_e, \tag{2}$$

where dN_e/dE_e is the number of energetic electrons [see Fig. 3(a)], d_C and n_C are the thickness of convertor and its atomic number density, respectively, and $E_{\rm cut}$ is the cutoff energy of the e^- beam.

We first consider the convertor material and thickness for efficient production of bremsstrahlung photons. Both Ta and Au plates can realize a high bremsstrahlung conversion efficiency owing to their large atomic numbers. However, Ta is cheaper than Au. With this consideration in mind, we choose a metallic Ta target as the bremsstrahlung convertor. A 2-mm-thick convertor, although not thick enough to give the peak yield of bremsstrahlung radiation, does lead to maximum production of ^{62,64}Cu. This is attributed to the fact that high-energy electrons penetrating the convertor effectively initiate extra production of the desired isotopes. A similar effect has been observed in the laser transmutation of nuclear ^{126}Sn waste.[27]

We further study the effect of plasma conditions on bremsstrahlung production. The simulation results are shown in Fig. 5. It can be seen that the bremsstrahlung production is most efficient at $n_e = 0.5n_c$ owing to the maximum production of high-energy electrons, as displayed in Fig. 4. When accounting for the photons in the energy region of GDR, we obtain a γ-beam flux of a few 10^{10} per laser shot. Since the broadband bremsstrahlung spectrum overlaps a significant part of the cross section on ^{63,65}Cu(γ, n) reactions, both of which are peaked at around 15 MeV (see Fig. 5), the required isotope production can be initiated efficiently in our scheme.

C. Photonuclear production of ^{62,64}Cu isotopes

For a typical photonuclear reaction, the production rate (yield) of the target isotopes depends upon the bremsstrahlung spectrum $n_\gamma(E_\gamma)$ and the cross section of the corresponding photonuclear reaction $\sigma_{\rm reac}(E_\gamma)$. Neglecting the attenuation of the photons in the target, the production rate can be written as

$$P_0 = N_{\rm re} \approx d_T n_T \int_{E_{\rm th}}^{E_{\rm max}} \sigma_{\rm reac}\left(E_\gamma\right) n_\gamma\left(E_\gamma\right) dE_\gamma, \tag{3}$$

where $E_{\rm th}$ is the threshold energy of the photonuclear reaction, $E_{\rm max}$ is the endpoint energy of the bremsstrahlung spectrum, and d_T and n_T are the thickness of the activation target and the number of activation target nuclei, respectively. In our simulation, a natural Cu target with an isotopic composition of ^{63}Cu (abundance 69.15%) and ^{65}Cu (30.85%) is employed to produce the ^{62,64}Cu isotopes. As already mentioned, both of these are medically relevant isotopes.

The influence of the target thickness on the production rate of ^{62,64}Cu isotopes is investigated. The production rate first increases significantly and then decreases slowly with increasing convertor thickness. The maximum production rate appears when the convertor

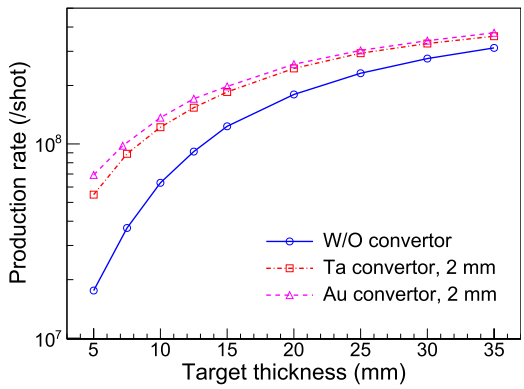

FIG. 6. Total production rate of ^{62,64}Cu isotopes as a function of the thickness of the activation target for different convertors. The plasma density is set to 0.5n_c.

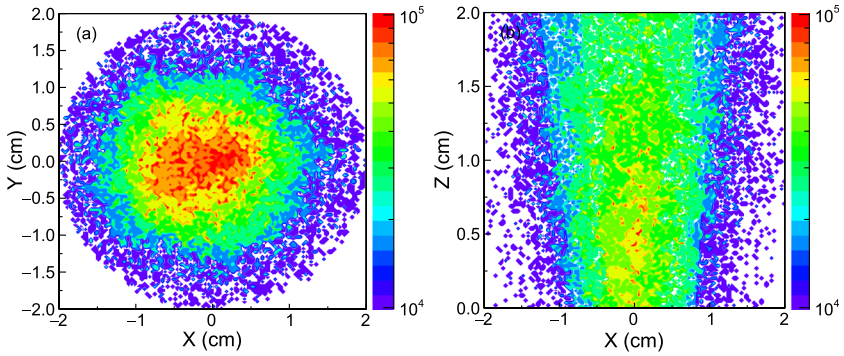

FIG. 7. Projected distributions of product nuclei ^{62,64}Cu in the *xy* and *xz* planes.

thickness is 2 mm. For different convertor materials, the production rate as a function of the thickness of the activation target is shown in Fig. 6. It can be seen that the production rate is increased significantly when the activation target is thinner than 20 mm. For thicker activation targets, the growth trend is not obvious, owing to the large attenuation of the bremsstrahlung radiation. When the convertor is absent, the collimated e^- beam directly irradiates the activation target, in which both the bremsstrahlung radiation and isotope production processes are initiated. However, the production rate of ^{62,64}Cu isotopes is visibly reduced (see Fig. 6).

To obtain a better understanding of the photonuclear processes induced by the energetic bremsstrahlung radiation, we examine the spatial distributions of the Cu isotopes. It can be seen from Fig. 7 that the intensity of the Cu isotopes decreases along both the radial and longitudinal directions, and the peak intensity is found in the center of the Cu target. The peak is also superposed closely on the incident γ-ray beam. Since, as already mentioned, the γ-ray beam has a small angular divergence, the intensity pattern induced by the photonuclear reactions is dispersed spatially along the direction of γ-beam propagation (see Fig. 7). One can see that the spatial pattern could provide information to help the choice of target geometry. In this case, a Cu target with 2 cm radius and thickness may satisfy the requirement for irradiation.

From target irradiation, a large number of neutrons, electrons, and γ-rays can be generated. Compared with the direct detection of these emitted particles, the activation measurement method can effectively alleviate the disturbance of these online backgrounds. Activity measurements on the radioactive residual nuclei produced by the (γ, n) reaction can be used for many isotopes. By using high-purity germanium (HPGe) detectors, the characteristic energy and decay-time pattern of the nuclear transitions can be measured precisely, allowing determination of the reaction yields[31] and hence the activity of the reaction products.

We simulate the detection of the characteristic γ-emissions (0.511 MeV) of ^{62,64}Cu and then analyze quantitatively the activity of the reaction products. An HPGe crystal of radius 29.6 mm, which is close to the front surface of the activation target, is employed in the simulation. Figure 8 shows the production and detection yields of ^{62,64}Cu as functions of the thickness of the activation target. The detection yield is obviously less than the production yield owing to attenuation of the characteristic γ-lines. When the target thickness exceeds 20 mm, the detection yield becomes saturated (see Fig. 8), which is in good agreement with the theoretical prediction. For the 0.511 MeV γ-rays attenuating inside the Cu target, the linear attenuation coefficient is 0.75 cm^{-1}. This value results in a half-attenuation thickness of 10 mm, indicating that the saturation thickness is of the order of 20 mm. From the simulation results shown in Figs. 7 and 8, we find that the

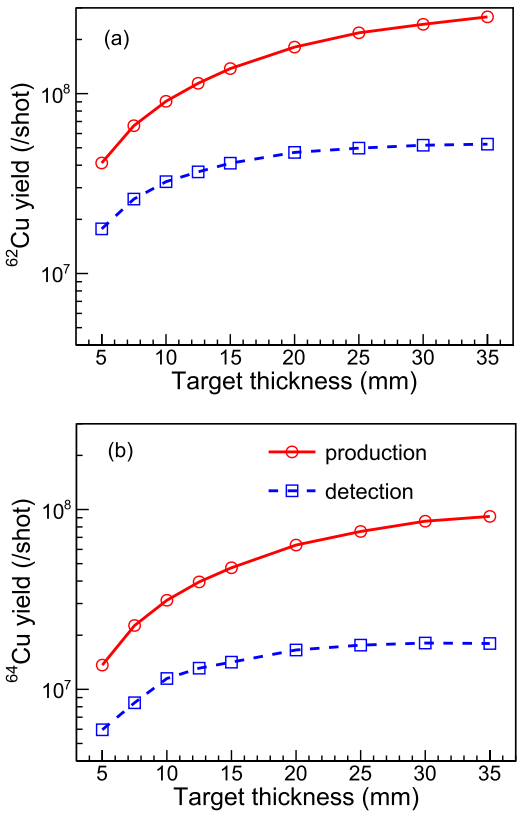

FIG. 8. Production and detection yields of ^{62,64}Cu isotopes as functions of the thickness of the activation target.

optimal radius and thickness of the activation target are both 20 mm.

The activity of the product isotope can be written as[32,33]

$$A_0 = P_0\left(1 - e^{-\lambda t_i}\right) \quad (4)$$

where $\lambda = \ln 2/\tau$ is the decay constant of the product isotope with a half-life of τ, and t_i is the irradiation time. The activities of ^{62,64}Cu isotopes for different plasma densities are calculated using the optimal irradiation parameters, and the results are shown in Fig. 9. One can see that the activities of the Cu isotopes are sensitive to the plasma density when this is below $0.3n_c$ or above $0.8n_c$. The activities of the medical isotopes are peaked at $n_e = 0.5n_c$. The activity level reaches 95% of the maximum (equilibrium) activity after an irradiation time corresponding to three half-lives of the products $3\tau_{Cu\text{-}62} = 0.5$ h and $3\tau_{Cu\text{-}64} = 38.1$ h. Corresponding activities of 0.18 GBq (4.9 mCi) for ^{62}Cu and 0.06 GBq (1.6 mCi) for ^{64}Cu are obtained. When the irradiation stops, the isotopes start to decay with their characteristic half-lives (indicated as cooling), which is also displayed in Fig. 9.

III. DISCUSSION

It can be seen that activities of 0.18 GBq for ^{62}Cu and 0.06 GBq for ^{64}Cu can be achieved using a sub-petawatt laser pulse (~350 TW) at 1 Hz repetition rate (see Fig. 9). In recent years, the development of laser technologies has provided the opportunity to produce compact high-repetition-rate systems.[34,35] In particular, the advanced laser at the University of Quebec, Canada[36] and the Diocles laser at the University of Nebraska–Lincoln, USA[37] have come online at a normal power level of 100 TW and 10 Hz. Furthermore, several laser facilities are being proposed to generate >1 PW power at a repetition rate of 10 Hz, such as the Mercury laser facility at the Lawrence Livermore National Laboratory (LLNL), USA.[38] For a sub-petawatt laser at 10 Hz to be used for ^{62,64}Cu isotope production, the resulting activity needs to be scaled proportionally to the order of gigabecquerels, which is at least one order of magnitude higher than what has previously been achieved (for production of the principal PET isotopes ^{11}C and ^{18}F).[20,21] Moreover, it is expected to reach the level of the activity required for PET imaging. Figure 10 summarizes our calculations of laser-driven ^{62,64}Cu isotope production via (γ, n) reactions, together with previous measurements of laser-driven ^{11}C and ^{18}F isotope production via (p, n) reactions. It can be seen that the potential of PET isotope production scales quantitatively with laser irradiance. It should be possible to generate an amount of activity of ^{62,64}Cu in 1 s that is equivalent to the required patient dose for PET, but not the greater amount of activity required for targeted radiotherapy. This extrapolation has been made with a great deal of caution, however, because experiments have yet to be performed at laser irradiances higher than 10^{21} W/cm^2.

The energy that is transferred to the target and the subsequent heating by the e^- or γ-ray beam may or not be sufficient to cause melting of the convertor, although this could be evaluated through additional calculations. However, for the specific cases considered in this study, Ta and Cu have melting points of 2996 °C and 1083.4 °C, respectively. Given these low melting points, to prevent excessive heating and avoid melting, it should be possible to use a multiple thin target experimental setup that allows the electrons and positrons produced by Compton scattering and by pair creation to leave the target rapidly, together with a water-cooling blanket.

Synthesis of Cu radiopharmaceuticals is another key issue with regard to clinical applications. It has been demonstrated that the 9.74 min half-life of generator-produced ^{62}Cu is long enough for synthesis of chemically diverse radiopharmaceuticals.[39] This should also be the case for laser-produced ^{62}Cu.

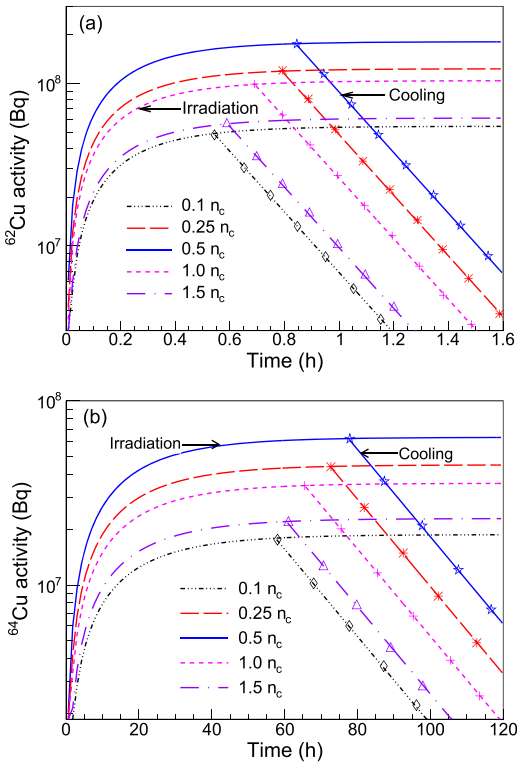

FIG. 9. Induced activities of ^{62,64}Cu isotopes for a wide range of plasma density. The activity during the cooling time is also shown as indicated. The radius and thickness of the activation target used in the simulations are both 20 mm.

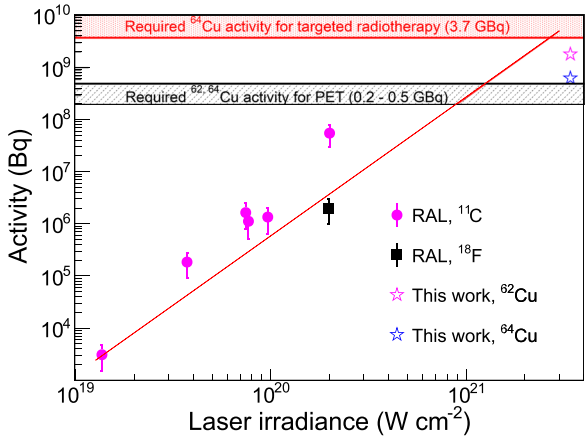

FIG. 10. Simulated and measured activities of a few PET isotopes as a function of laser irradiance. The laser specifications for the RAL measurements are given in Ref. 21. For comparison, all data are given for a laser repetition rate of 10 Hz.

IV. CONCLUSIONS

We have illustrated by simulations the laser production of ^{62,64}Cu isotopes through photonuclear reactions. A collimated relativistic e^- beam with a high charge of approximately 100 nC, produced by the interaction of a high-intensity laser with an NCD plasma, can generate high-flux (10^{10} per laser shot) bremsstrahlung γ-rays in the GDR region. Normally, an argon gas jet is used in experiments to generate NCD plasmas.[40] The plasma density and target geometry are optimized to enhance the production yields of ^{62,64}Cu isotopes. The possibility of detecting the activity of ^{62,64}Cu isotopes has also been presented. This study shows that very intense sources of ^{62,64}Cu with activity reaching the levels required for PET can be obtained by employing state-of-the-art laser systems. We further expect that laser production will also be suitable for other isotopes of medical interest, such as ^{68}Ga, ^{186}Re, and ^{225}Ra.

ACKNOWLEDGMENTS

This work is supported by the National Natural Science Foundation of China (Grant No. 11675075) and the Natural Science Foundation of Hunan Province, China (Grant No. 2018JJ2315). W.L. appreciates support from the Youth Talent Project of Hunan Province, China (Grant No. 2018RS3096).

REFERENCES

[1]D. Habs and U. Köster, "Production of medical radioisotopes with high specific activity in photonuclear reactions with γ-beams of high intensity and large brilliance," Appl. Phys. B **103**(2), 501–519 (2011).
[2]M. Bobeica, D. Niculae *et al.*, "Radioisotope production for medical applications at ELI-NP," Rom. Rep. Phys. **68**(Suppl), 847–883 (2016).
[3]W. Luo, "Production of medical radioisotope Cu-64 by photoneutron reaction using ELI-NP γ-ray beam," Nucl. Sci. Technol. **27**(4), 96 (2016).
[4]P. J. Blower *et al.*, "Copper radionuclides and radiopharmaceuticals in nuclear medicine," Nucl. Med. Biol. **23**(8), 957–980 (1996).
[5]K. R. Zinn, T. R. Chaudhuri *et al.*, "Production of no-carrier-added ^{64}Cu from zinc metal irradiated under boron shielding," Cancer **73**(S3), 774–778 (1994).
[6]J. Y. Kim *et al.*, "A simple Cu-64 production and its application of Cu-64 ATSM," Appl. Radiat. Isot. **67**(7-8), 1190–1194 (2009).
[7]J. Kozempal, K. Abbas, F. Simonelli *et al.*, "A novel method for n. γ. a. ^{64}Cu production by the ^{64}Zn(d, 2p)^{64}Cu reaction and dual ion-exchange column chromatography," Radiochim. Acta **95**(2), 75–80 (2007).
[8]J. B. Philip *et al.*, "Copper radionuclides and radiopharmaceuticals in nuclear medicine," Nucl. Med. Biol. **23**, 957–980 (1996).
[9]Y. Fujibayashi *et al.*, "A new zinc-62/copper-62 generator as a copper-62 source for PET radiopharmaceuticals," J. Nucl. Med. **30**(11), 1838–1842 (1989).
[10]A. G. Mark, "Copper-62 radiopharmaceuticals for diagnistic imaging with position emission tomography (PET)," Transition Met. Chem. **22**, 427 (1997).
[11]T. Fukumura, K. Okada *et al.*, "An improved ^{62}Zn/^{62}Cu generator based on a cation exchanger and its fully remote-controlled preparation for clinical use," Nucl. Med. Biol. **33**(6), 821–827 (2006).
[12]W. Luo, M. Bobeica, D. Filipescu *et al.*, "Production of radioisotopes of medical interest by photonuclear reaction using ELI-NP γ-ray beam," Acta Phys. Pol. B **47**(3), 763–769 (2016).
[13]P. Gould, "Medical isotope shortage reaches crisis level," Nature **460**(7253), 312–313 (2009).
[14]V. Noorden and R. Radioisotopes, "The medical testing crisis," Nature **504**(7479), 202–204 (2013).
[15]C. Danson, D. Hillier, N. Hopps *et al.*, "Petawatt class lasers worldwide," High Power Laser Sci. Eng. **3**, e3 (2015).
[16]G. A. Mourou, C. L. Labaune, M. Dunne *et al.*, "Relativistic laser-matter interaction: From attosecond pulse generation to fast ignition," Plasma Phys. Controlled Fusion **49**(12B), B667 (2007).
[17]G. A. Mourou, T. Tajima, and S. V. Bulanov, "Optics in the relativistic regime," Rev. Mod. Phys. **78**(2), 309 (2006).
[18]K. W. D. Ledingham, P. McKenna, and R. P. Singhal, "Applications for nuclear phenomena generated by ultra-intense lasers," Science **300**(5622), 1107–1111 (2003).
[19]W. Qi, Y. Q. Gu *et al.*, "Enhanced photoneutron production by intense picoseconds laser interacting with gas-solid hybrid targets," Phys. Plasmas **26**, 043103 (2019).
[20]S. Fritzler, V. Malka, G. Grillon *et al.*, "Proton beams generated with high-intensity lasers: Applications to medical isotope production," Appl. Phys. Lett. **83**(15), 3039–3041 (2003).
[21]K. W. D. Ledingham, P. McKenna, T. McCanny *et al.*, "High power laser production of short-lived isotopes for positron emission tomography," J. Phys. D: Appl. Phys. **37**(16), 2341 (2004).
[22]C. P. Ridgers, J. G. Kirk, R. Duclous *et al.*, "Modelling gamma-ray photon emission and pair production in high-intensity laser–matter interactions," J. Comput. Phys. **260**, 273–285 (2014).
[23]S. Agostinelli, J. Allison, K. Amako *et al.*, "GEANT4-a simulation toolkit," Nucl. Instrum. Methods Phys. Res., Sect. A **506**(3), 250–303 (2003).
[24]W. Luo, H. Y. Lan, Y. Xu *et al.*, "Implementation of the n-body Monte-Carlo event generator into the Geant4 toolkit for photonuclear studies," Nucl. Instrum. Methods Phys. Res., Sect. A **849**, 49–54 (2017).
[25]A. Modena *et al.*, "Electron acceleration from the breaking of relativistic plasma waves," Nature **377**, 606 (1995).
[26]R. Hu, B. Liu, H. Lu *et al.*, "Dense helical electron bunch generation in near-critical density plasmas with ultrarelativistic laser intensities," Sci. Rep. **5**, 15499 (2015).
[27]X. L. Wang, Z. Y. Xu, W. Luo *et al.*, "Transmutation prospect of long-lived nuclear waste induced by high-charge electron beam from laser plasma accelerator," Phys. Plasmas **24**(9), 093105 (2017).
[28]X. L. Wang, Z. Y. Tan, W. Luo *et al.*, "Photo-transmutation of long-lived radionuclide ^{135}Cs by laser–plasma driven electron source," Laser Part. Beams **34**(3), 433–439 (2016).
[29]E. Irani, H. Omidvar, and R. Sadighi-Bonabi, "Gamma rays transmutation of Palladium by bremsstrahlung and laser inverse Compton scattering," Energy Convers. Manage. **77**, 558–563 (2014).
[30]V. V. Varlamov, A. I. Davydov, M. A. Makarov *et al.*, "Reliability of the data on the cross sections of the partial photoneutron reaction for ^{63,65}Cu and ^{80}Se nuclei," Bull. Russ. Acad. Sci.: Phys. **80**(3), 317–324 (2016).
[31]K. M. Spohr, M. Shaw, W. Galster *et al.*, "Study of photo-proton reactions driven by bremsstrahlung radiation of high-intensity laser generated electrons," New J. Phys. **10**(4), 043037 (2008).
[32]W. Luo, D. L. Balabanski, and D. Filipescu, "A data-based photonuclear simulation algorithm for determining specific activity of medical radioisotopes," Nucl. Sci. Tech. **27**(5), 113 (2016).
[33]W. Luo, M. Bobeica *et al.*, "Estimates for production of radioisotopes of medical interest at extreme light infrastructure–nuclear physics facility," Appl. Phys. B **122**(1), 8 (2016).
[34]R. Zhang, X. Tian, D. Zhou *et al.*, "Single-mode millijoule fiber laser system with high pulse shaping ability," Optik **157**, 1087–1093 (2018).
[35]A. Klenke *et al.*, "Coherently combined 16-channel multicore fiber laser system," Opt. Lett. **43**, 1519 (2018).
[36]S. Fourmaux, S. Payeur *et al.*, "Laser beam wavefront correction for ultra-high intensities with the 200 TW laser system at the advanced laser light source," Opt. Express **16**(16), 11987–11994 (2008).
[37]C. Liu, S. Banerjee, J. Zhang *et al.*, "Repetitive petawatt-class laser with near-diffraction-limited focal spot and transform-limited pulse duration," Proc. SPIE **8599**, 859919 (2013).
[38]M. D. Perry, D. Pennington, B. C. Stuart *et al.*, "Petawatt laser pulses," Opt. Lett. **24**(3), 160–162 (1999).
[39]N. G. Haynes *et al.*, "Performance of a ^{62}Zn/^{62}Cu generator in clinical trials of PET perfusion agent ^{62}Cu-PTSM," J. Nucl. Med. **41**, 309–314 (2000).
[40]T. J. Xu, B. F. Shen *et al.*, "Ultrashort megaelectronvolt positron beam generation based on laser-accelerated electrons," Phys. Plasmas **23**(3), 033109 (2016).